Materials Science and Engineering: A (2013). 580, 142-149.
DOI: http://dx.doi.org/10.1016/j.msea.2013.04.071

Hot deformation behavior and workability characteristics of AZ91 magnesium alloy powder compacts—A study using processing map

M.A. Jabbari Taleghani [a,b,*], J.M. Torralba [a,b]

[a] Department of Materials Science and Engineering, Universidad Carlos III de Madrid, Avda. de la Universidad 30, 28911 Leganés, Madrid, Spain

[b] IMDEA Materials Institute, C/Eric Kandel 2, Tecnogetafe, 28906 Getafe, Madrid, Spain

* Tel.: +34 91 5493422; fax: +34 91 5503047. E-mail addresses: mohammad.jabbari@imdea.org, mo.jabbari@yahoo.com (M.A. Jabbari Taleghani).

Abstract: This study examined the hot deformation behavior and workability characteristics of AZ91 Mg alloy powder compacts by performing hot compression tests with a Gleeble 3800 machine. To this end, powder compacts with a relative green density of 93% were hot-compressed at temperatures ranging from 150 °C t o 5 0 0 °C and at true strain rates ranging from 0.001 s^{-1} to 10 s^{-1}. The true stress–true strain curves peaked at low strains, after which the flow stress increased slightly or remained constant. The work hardening rate decreased with increasing deformation temperature or strain rate. Processing maps were developed for all of the hot compression tests at strains of 0.1, 0.5, and 0.8, which represented a safe deformation domain at deformation temperatures and strain rates in the ranges of 150–300 °C and 0.001–0.01 s^{-1}. Kinetic analysis of the flow stress data for the safe deformation domain yielded an activation energy of 75 kJ/mol which is lower than those previously reported for the hot compression of bulk AZ91 Mg alloy. According to the developed processing maps and the microstructures of the hot-compressed specimens, the optimum hot working window for AZ91 Mg alloy powder compacts was determined to lie between 275–325 °C and 0.001–0.01 s^{-1}.

Keywords: AZ91 magnesium alloy, Pre-alloyed powder, Hot deformation behavior, Processing map, Workability

1. Introduction

Having a density of 1.74 g/cm^3, Mg is considered as the lightest engineering metal available. It is 35% lighter than aluminum (2.7 g/cm^3) and over four times lighter than iron (7.87 g/cm^3) [1,2]. Mg alloys have received considerable attention as a structural material in recent years due to their interesting properties, such as low density, high strength-to-weight ratio, good damping characteristics, superior machinability, and excellent castability [3–5]. Besides, Mg is a very promising candidate for biocompatible and biodegradable applications in modern medicine [6]. Most of the research and development on these alloys has been performed by the automotive industry; and die casting has been the main manufacturing route for Mg products because of the poor workability of Mg at room temperature, which is a result of its HCP crystal structure [7,8]. However, Mg die cast products have considerable disadvantages, such as pin holes, porosity, cold shuts and low strength. Moreover, die cast products do not meet the required dimensional tolerances for precision parts and must be heavily machined prior to use [9]. In fact, the market for Mg products continues to grow; but many opportunities remain untapped because of the relatively low stiffness and strength of these products. Fabrication by plastic forming at elevated temperatures has considerable potential for Mg alloys because the worked alloys have greater strength and ductility than the castings [10,11].

Mg powder metallurgy combines the superior properties of Mg with the advantages of powder metallurgy (PM) to produce high-performance, net- or near-net-shaped parts, thus alleviating the formability problem of Mg and its alloys and reducing or eliminating the capital and operating costs associated with intricate machining operations. The surfaces of the Mg-based powders are covered with a stable oxide layer of 3–5 nm, which strongly inhibits sintering of these powders. Hence, the sintering of Mg-based powders is generally regarded as unfeasible and problematic [6]. Powder extrusion (PE) and powder forging (PF) are PM processing methods that have been developed for the production of fully dense, high-performance bulk materials from powder mixtures. Compared with other PM routes such as sintering and hot pressing (HP), the shear stresses involved in PE and PF make them ideal processes for the production of bulk Mg products from powder mixtures. These shear stresses can break the oxide layer covering the surfaces of Mg-based powder particles, which results in a well-bonded microstructure and superior after-consolidation mechanical properties [12]. Furthermore, it is a well-known fact that the mechanical properties of Mg alloys can be effectively improved by refining their grain structures through

recrystallization, which generally occurs during hot deformation of these materials. Due to the limited number of slip systems of Mg and its correspondingly large Taylor factor, grain refinement remarkably improves the mechanical properties of both Mg and its alloys. The fabrication of diverse Mg products using hot plastic forming processes, such as extrusion, forging, and rolling, can increase the consumption of Mg and its alloys [4].

A good understanding of the hot deformation behavior of a material is extremely important in hot deformation processes such as extrusion and forging [13–15]. Processing parameters, such as deformation temperature and strain rate, and material factors, such as microstructure of the starting material, are the main factors affecting the hot deformation flow stress. Thus, several studies have been performed to investigate the effect of both processing parameters and materials factors on the hot deformation behavior of bulk Mg alloys [11,16–18]. The deformation behavior of porous materials is different from that of bulk materials. Pores present in the microstructure act as stress concentration points, limiting the amount of deformation to fracture [19,20]. Moreover, the volume of voids is reduced during deformation, which results in an increase in density and densification. In addition to strain hardening, densification during deformation can enhance the flow stress of the material, which is known as densification hardening [21]. In the case of powder-based porous materials, such as powder compacts, due to friction between particles, redundant work is required to weld powder particles together, break welds between particles, and re-weld them together [12]. Thus, information on the deformation behavior of bulk Mg alloys may not be completely usable for the deformation of porous alloys with similar chemical compositions. Nevertheless, there are almost no systematic studies on the hot deformation behavior of porous Mg alloys.

Among all of the existing Mg alloys, AZ91 is the most widely used alloy in the industry [10,22]. Some researchers have successfully applied hot deformation processes, such as hot compression [23], extrusion [24], equal channel angular pressing (ECAP) [25], and hot rolling [26], to as-cast AZ91 alloy and improved its mechanical properties to broaden the application potential for this alloy. However, studies on the hot deformation behavior of AZ91 alloy are relatively scarce [27,28]; and very limited data are available on this alloy's workability characteristics. Therefore, this study focused on the hot deformation behavior and workability characteristics of AZ91 Mg alloy powder compacts with a view to finding the optimum hot working parameters. For this purpose, the approaches of processing map and kinetic analysis have been adopted.

The processing map technique used in this study is based on the dynamic materials modeling (DMM), and the efficiency of the power dissipation (η) through microstructural changes during deformation is given by [18,29]

$$\eta = 2m/(m+1) \tag{1}$$

where m is the strain rate sensitivity of flow stress given by "$(\partial \log \dot{\varepsilon})/(\partial \log \sigma)$". The extremum principles of irreversible thermodynamics as applied to the continuum mechanics of large plastic flow were explored to define a criterion for the onset of flow instability, given by

$$\xi = (\partial \ln[m/(m+1)]/\partial \ln \dot{\varepsilon}) + m \leq 0 \tag{2}$$

The standard kinetic rate equation relating the flow stress (σ) to strain rate ($\dot{\varepsilon}$) and deformation temperature (T) is given by

$$\dot{\varepsilon} = A\sigma^n \exp(-Q/RT) \tag{3}$$

where A is a constant, n is the stress exponent, Q is the activation energy of hot deformation (J/mol), R is the gas constant (8.31 J mol^{-1} K^{-1}), and T is the absolute temperature (K).

2. Experimental procedure

The raw material used for this study was a pre-alloyed Mg–Al–Zn powder (Ecka Granules, Germany) with a chemical composition equivalent to that of AZ91 D alloy (8.8 wt% Al, 0.6 wt% Zn, 0.2 wt% Mn, 0.03 wt% Si, and the balance Mg). Fig. 1 illustrates the morphology and particle size distribution of the as-received powder, showing that the powder particles possess the irregular, plate-like morphology that is typical of Mg-based powders produced by the mechanical grinding of casting ingots. The average particle size ($D_{0.5}$) of the powder was measured to be 100 μm.

The above mentioned powder was uniaxially cold pressed at 600 MPa into cylindrical billets measuring 10 mm in diameter and 15 mm in height using no pressing lubricant. The green densities of the powder compacts were measured to be 93% of the theoretical value, or 1.81 g/cm^3.

A graphite foil with a thickness of 0.05 mm was placed between the ends of the powder compacts and the anvils to minimize friction during the hot compression test. Prior to the hot compression tests, the samples were resistance heated in an Ar atmosphere to the required temperature at a heating rate of 3 °C s^{-1}, then maintained at the test temperature for 1 min to minimize thermal gradients along the sample. Single-hit compression tests were

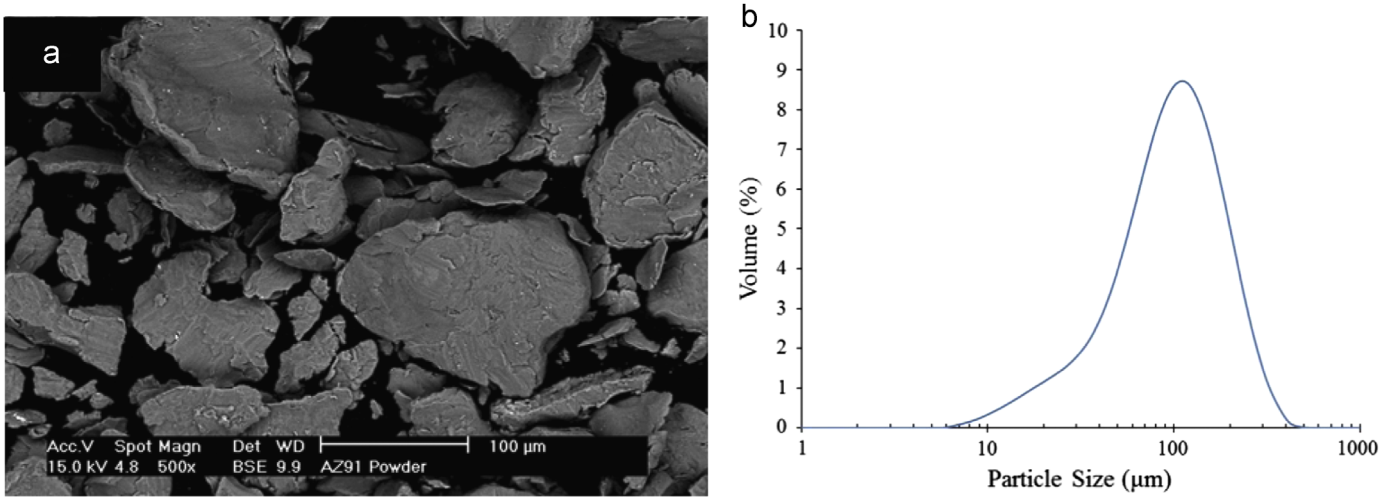

Fig. 1. (a) Morphology and (b) particle size distribution of the as-received AZ91 powder.

performed using a servo-controlled Gleeble-3800 system (Dynamic Systems Inc, USA) at strain rates of 0.001 s^{-1}, 0.01 s^{-1}, 0.1 s^{-1}, 1 s^{-1}, and 10 s^{-1} and deformation temperatures ranging from 150 °C to 500 °C, which cover the entire hot working range of Mg alloys. The specimens were deformed to a true strain of 0.8. After hot compression, the samples were air-quenched to room temperature. The load-stroke data were converted into true stress–true strain curves using standard equations, which in turn used to compute the efficiency (η) and instability (ξ) parameters as a function of temperature and strain rate.

The hot-compressed specimens were sectioned in the center parallel to the compression direction for the microstructural analysis. The sectioned samples were then mounted, ground, polished, and examined using optical microscopy (OM) and scanning electron microscopy (SEM). Several samples were also etched using acetic acid etchant (5 ml acetic acid, 95 ml water) prior to optical imaging.

3. Results and discussion

3.1. Starting microstructure

Fig. 2(a) illustrates the cross-section microstructure of an AZ91 Mg alloy powder compact, showing that the microstructure of AZ91 powder particles was comprised of a dark gray matrix in which some gray phases were randomly distributed. The EDS analyses (data not shown) determined that the dark gray matrix was enriched in Mg while the gray precipitates were enriched in Mg and Al. As the atomic numbers of Mg and Al are 12 and 13 respectively, SEM in backscattered electron (BSE) mode was not capable of making an obvious contrast between the matrix of powder particles and the precipitates containing Al. As a result, these precipitates are highlighted using black ovals. The XRD pattern of the as-received AZ91 powder is presented in Fig. 2(b). As shown, the microstructure of AZ91 powder particles was composed of the α-Mg solid solution phase (the dark gray matrix of the powder particles) and the β-$Mg_{17}Al_{12}$ precipitates, i.e. the gray precipitates in Fig. 2(a). This structure is typical of AZ91 castings.

AZ Mg casting alloys with a high content of Al normally contain a large amount of β precipitates, which form during solidification of these alloys. The β precipitates are generally considered to have detrimental effects on mechanical properties and workability of AZ Mg alloys. Therefore, casting ingots of AZ Mg alloys are usually subjected to a solution treatment (heating to 415 °C and holding at this temperature for 12–24 h) prior to any thermo-mechanical processing [30]. However, some researchers believe that the β precipitates may be beneficial to the hot deformation of AZ Mg alloys [31]. In addition, elimination of the solution treatment and direct use of the as-cast alloy for hot deformation can significantly decrease the manufacturing cost of AZ Mg alloys wrought products [32]. Considering all above, for this study no solution treatment was performed on AZ91 Mg alloy powder compacts prior to hot compression.

Unlike Al, most of the commercial Mg-based powders are produced by mechanical grinding of as-cast ingots. As a result, the constituent phases of these powders are similar to those of the parent ingots. Powders produced by mechanical grinding have an angular morphology (Fig. 1(a)). Due to the mechanical interlocking, this morphology results in a good green strength. However, the layer covering the surfaces of Mg-based powders produced by mechanical grinding is typically thicker than that covering the surface of atomized powders [33].

3.2. Flow stress curves

The true stress–true strain curves obtained at deformation temperatures of 200 °C, 350 °C, and 450 °C and at different strain rates are shown in Fig. 3(a), (b), and (c), respectively, and represent typical deformation behavior at low (T≤200 °C), moderate (250 °C≤T≤400 °C), and high deformation temperatures (450 °C≤T).

The specimens cracked severely or fragmented at every test temperature and a strain rate of 10 s^{-1}, resulting in a sharp or gradual drop in the flow stress after its peak. The specimens again cracked severely or fragmented at a strain rate of 1 s^{-1} and both low and high deformation temperatures. Specimen cracking also occurred at a strain rate of 1 s^{-1} and moderate temperatures, although it is not reflected in the specimens' flow stress curves. The true stress–true strain curves exhibited a peak at strain rates less than or equal to 0.1 s^{-1}, after which the flow stress increased slightly or remained nearly constant. As the deformation temperature increased or the strain rate decreased, a decrease in the peak stress level was observed. Moreover, a higher deformation temperature or strain rate resulted in a lower work hardening rate. At a deformation temperature of 450 °C, the flow behavior at a strain rate of 0.1 s^{-1} was similar to that at strain rates of 1 s^{-1} and 10 s^{-1}, suggesting that the cracking phenomenon was more critical at higher deformation temperatures than at lower temperatures.

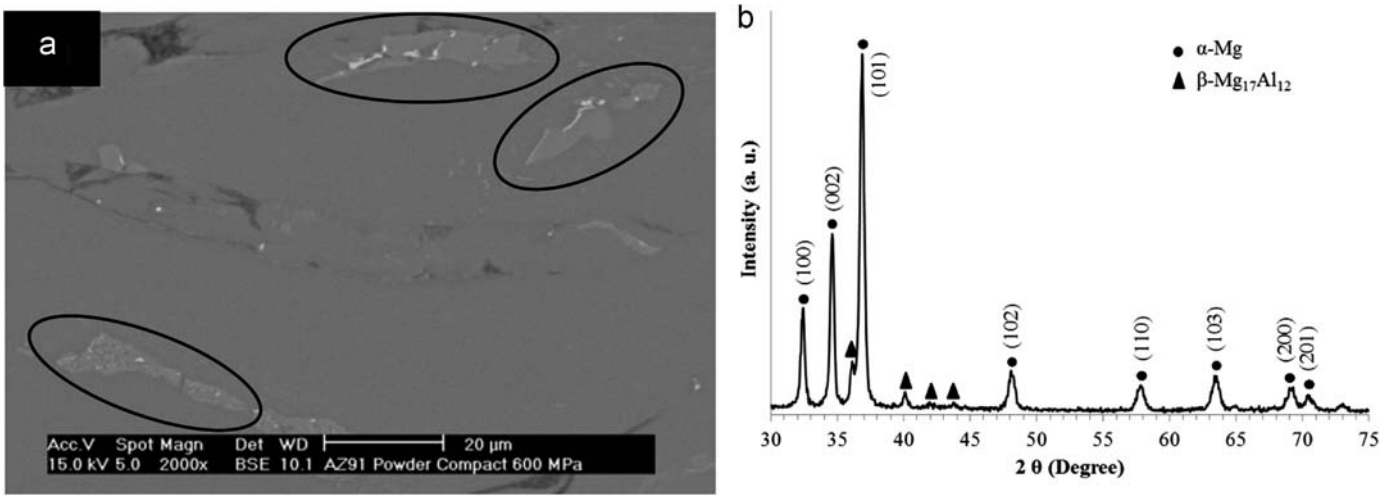

Fig. 2. (a) Cross-section microstructure and (b) XRD pattern of the as-received AZ91 powder.

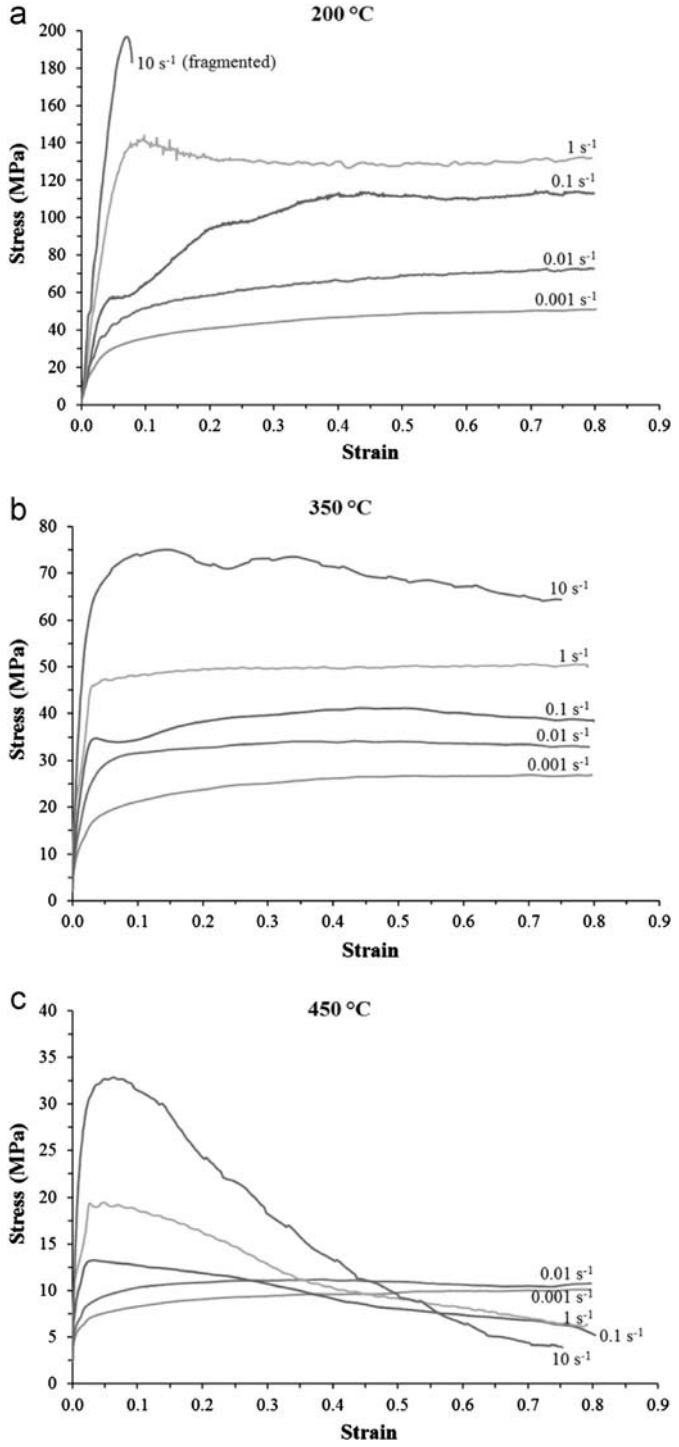

Fig. 3. True stress–true strain curves of the AZ91 Mg alloy powder compacts hot-compressed at deformation temperatures of (a) 200 °C, (b) 350 °C, and (c) 450 °C and at different strain rates.

During the deformation of porous materials at high temperatures, hardening mechanisms, such as strain and densification hardening, and softening mechanisms, such as dynamic recovery and recrystallization, can occur simultaneously. At the beginning of deformation, the dislocation density increases rapidly, which leads to a sharp increase in the flow stress [34]. As deformation continues, the activation of dynamic softening mechanisms can partially or completely neutralize the effect of hardening mechanisms. As a result, the slope of the flow stress flattens and may even become zero or negative.

3.3. Processing maps

The processing maps developed for strains of 0.1, 0.5, and 0.8 are shown in Fig. 4. The contour numbers in these figures

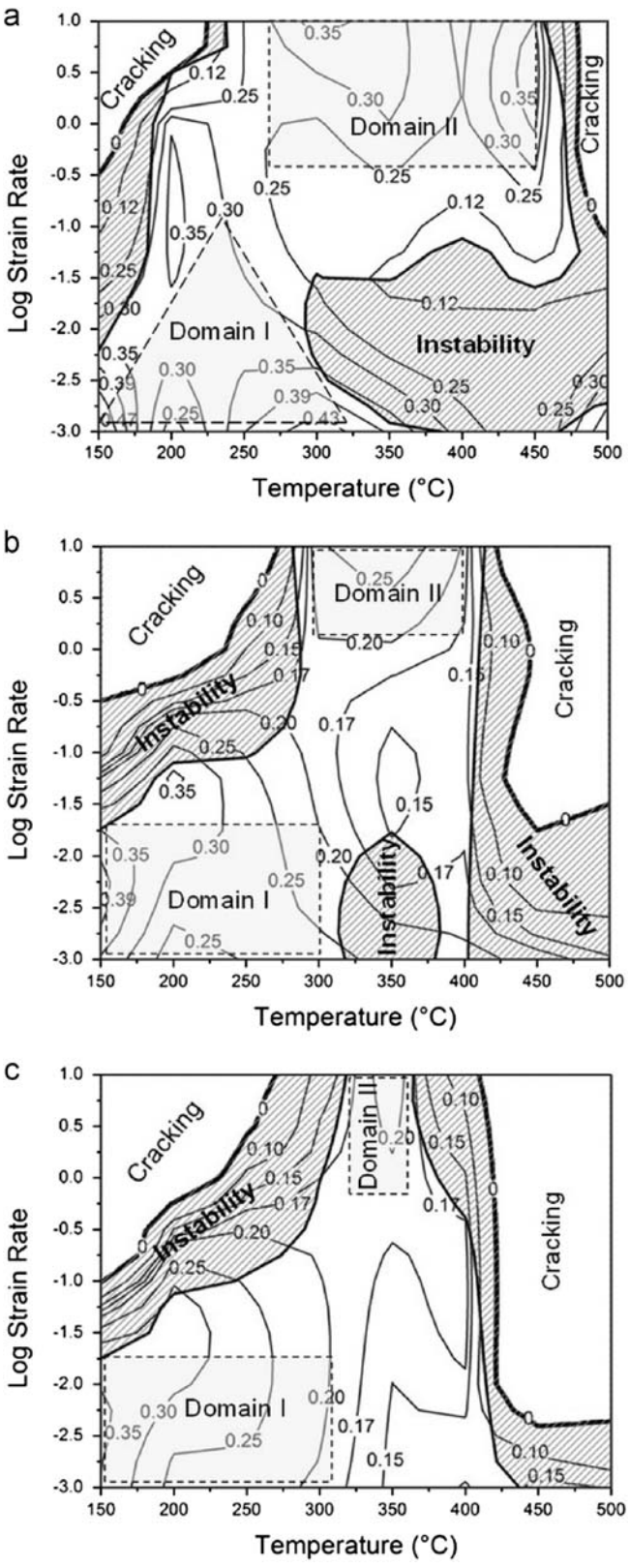

Fig. 4. Processing maps of the AZ91 Mg alloy developed at strains of (a) 0.1, (b) 0.5, and (c) 0.8.

represent the efficiency of the power dissipation through dynamic metallurgical mechanisms (η); and the hatched regions represent regions of flow instability, where the instability parameter (ξ) is negative. The regions labeled "Cracking" correspond to regions with negative η values that resulted from the severe cracking or fragmentation of the specimens during compression testing. Although the features of the three maps are basically similar, the alteration and expansion of instability and cracking regions with increasing strain suggest that strain has an important effect on the processing maps of AZ91 Mg alloy powder compacts.

As shown in Fig. 4, all of the processing maps include two cracking regions located at higher strain rates and both low and high deformation temperatures. Both regions expand significantly with increasing strain. The increase in strain also affects the instability regions. The instability region located at higher strain rates and low deformation temperatures expands with increasing strain. This expansion is particularly noticeable for "Log strain rate" greater than −0.5 (strain rates greater than 0.3 s^{-1}). However, the increase in strain has a different effect on the instability region located at high deformation temperatures. At "Log strain rate" less than or equal to −1.5 (strain rates less than or equal to 0.03 s^{-1}), this instability region significantly shrinks toward higher deformation temperatures with increasing strain. On the contrary, at "Log strain rate" greater than −1.5 (strain rates greater than 0.03 s^{-1}), the increase in strain slightly expands the instability region. This expansion is more noticeable for "Log strain rate" greater than −0.5 (strain rates greater than 0.3 s^{-1}), and the instability region extends toward moderate deformation temperatures. Fig. 4 clearly shows that the workability of AZ91 Mg alloy is not good at low and high deformation temperatures. Consequently, cracking and instability regions located at these temperatures expand with increasing strain. This expansion, in turn, affects the domains with high efficiency of the power dissipation (η). Then, the effect of strain on these domains is of great importance and should also be studied.

The processing map developed for a strain of 0.1 (Fig. 4(a)) exhibits two domains with high efficiency of the power dissipation (η). These domains are normally considered as the suitable conditions for hot deformation. Domain I shrinks slightly with increasing strain (Fig. 4(b) and (c)). However, strains greater than 0.5 do not show any shrinking effect on this domain, and domain I is basically similar for the processing maps developed for strains of 0.5 and 0.8. In contrast to domain I, the increase in strain greatly affects domain II. Both the area and the peak efficiency of domain II decrease noticeably with increasing strain. As shown in Fig. 4(c), the two instability regions surrounding domain II are about to merge and to dissolve this domain. Considering the effect of strain on domain II, this domain cannot be considered as a safe and suitable domain for the hot deformation of AZ91 Mg alloy powder compacts.

The map depicting a strain of 0.8 (Fig. 4(c)) exhibits a single domain of stable flow (Domain I) with a peak efficiency of about 35% in the following temperature and strain rate ranges: 150–300 °C and 0.001–0.01 s^{-1}, which is considered as the appropriate hot deformation window for AZ91 Mg alloy powder compacts. This map also contains large flow instability and cracking regions at both low and high deformation temperatures. These regions are not suitable for hot working of the material. Considering the incipient melting and solidus temperatures of the AZ91 Mg alloy, which are 420 °C and 470 °C, respectively, the alloy's poor workability at high deformation temperatures can be attributed to the negative effect of the melting phenomenon on the material's deformability.

Side views of the specimens hot-compressed at different temperatures and strain rates to a strain of 0.8 are presented in Fig. 5. The specimens experienced inhomogeneous deformation (i.e., flow localization) and/or cracking in the instability regions (the intensity of which increased with increasing strain rate) and severely cracked or fragmented in the cracking regions. The AZ91 alloy exhibited good workability within domain I and produced crack-free, uniformly deformed specimens, suggesting that the developed processing maps successfully identified the safe domain for the hot deformation of AZ91 Mg alloy powder compacts. As expected, the specimens deformed within domain II exhibited unacceptable surface quality and cracking.

The stress–strain curves obtained for domain I featured flow hardening behavior with a low hardening rate. During the hot deformation of porous materials such as the powder compacts under study, flow hardening mechanisms such as strain and densification hardening occur simultaneously. The latter mechanism results from a continuous increase in density during deformation. Furthermore, domains such as domain I that possess a high efficiency of the power dissipation (η) and good workability have generally been associated with dynamic restoration mechanisms, such as dynamic recovery and recrystallization [18]. At the beginning of deformation, the dislocation density and the density of the powder compact increase rapidly, which lead to a sharp increase in the flow stress. However, as deformation continues, the activation of dynamic restoration mechanisms neutralizes the effect of hardening mechanisms. Consequently, the slope of the true stress–true strain curve flattens and deformation continues with a lower work hardening rate.

3.4. Kinetics of hot deformation

The kinetic rate equation (Eq. (3)) is normally obeyed in the deterministic domains of the processing map [35,36]. The variation of the flow stress at a strain of 0.1 (near peak flow stress) with strain rate on a natural logarithmic scale is shown in Fig. 6(a). The average slope of the straight-line fits obtained at the temperatures and strain rates covering domain I of the processing map developed for a strain of 0.1 was considered to be an estimate of the value of m (the strain rate sensitivity of flow stress) for the mentioned domain. Then, this value was used to calculate the value of n ($=1/m$, the stress exponent in Eq. (3)). The value of n was determined to be 5.3 for domain I.

The value of "*Ln* (flow stress)" at a strain of 0.1 as a function of "1000/*T*" (*T*: absolute deformation temperature) is shown in Fig. 6(b). The average slope of the straight-line fits obtained at the temperatures and strain rates covering domain I of the processing map developed for a strain of 0.1 was used to calculate the value of Q (the activation energy of hot deformation) for this domain. The value of Q obtained from Fig. 6(b) was 75 kJ/mol, which is significantly lower than those previously reported for the hot compression of bulk AZ91 Mg alloy [9,27]. This can primarily be attributed to the presence of pores in the structure of AZ91 powder compacts. Q is an indicator of the degree of difficulty of deformation. Namely, as the deformation activation energy increases, deformation becomes more difficult. The presence of pores in the structure of porous materials reduces their resistance to deformation [20]. Consequently, a powder compact has a lower Q value than the bulk alloy with similar chemical composition and microstructure.

It should also be considered that the value of Q has dependences on many other factors, such as temperature range, alloy composition, and the starting microstructure. In the previous studies on hot deformation behavior of bulk AZ91 Mg alloy, the alloy was solutionized prior to hot compression [9,27]. Then, the alloying elements present in the chemical composition of AZ91 alloy, namely Al and Zn, can rationally be treated as mostly dissolved in the α-Mg solid solution phase. However, in this study no solution treatment was performed on AZ91 Mg alloy powder compacts before hot compression tests, and microstructure of the

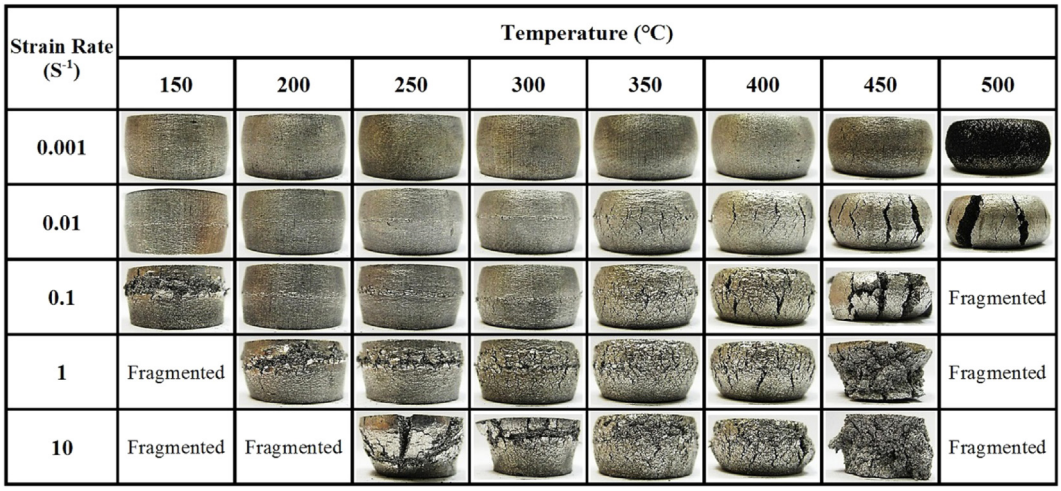

Fig. 5. Side views of the specimens hot-compressed at different temperatures and strain rates to a strain of 0.8.

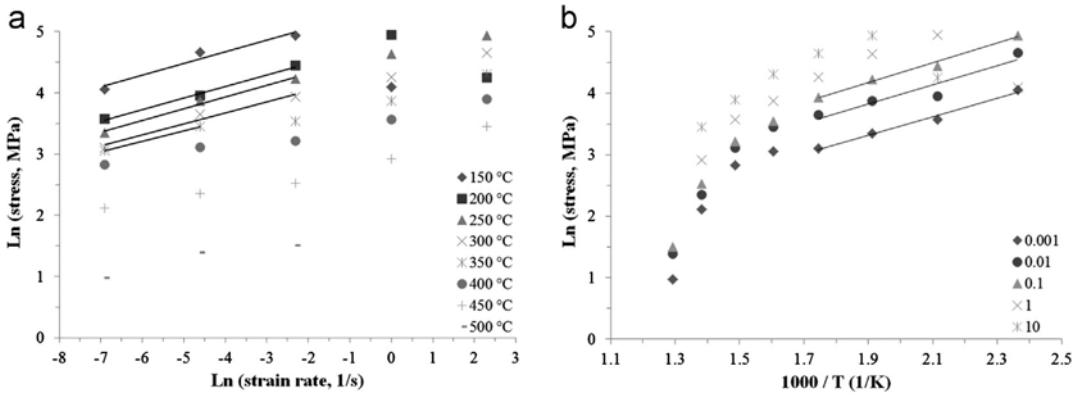

Fig. 6. (a) Variation of flow stress (strain 0.1) with strain rate on a natural logarithmic scale for the AZ91 Mg alloy powder compacts. (b) Arrhenius plot showing the variation of flow stress (strain 0.1) with inverse of absolute deformation temperature for the AZ91 Mg alloy powder compacts.

mentioned compacts was composed of the β-$Mg_{17}Al_{12}$ precipitates and the α-Mg solid solution phase. In other words, instead of being in solution, a large quantity of the alloying elements was out of the structure of α-Mg solid solution phase, forming the β-$Mg_{17}Al_{12}$ precipitates. Consequently, the lower Q value obtained in this study can partly be attributed to the initial microstructure of AZ91 Mg alloy powder compacts. It is believed that the content of alloying elements in solution has an important effect on the Q value of AZ series Mg alloys and the Q value of this alloy series increases with the increasing content of Al in solution (dissolved in the α-Mg solid solution phase). This phenomenon can be ascribed to the solute dragging effect of Al atoms in solution and the precipitation of fine β particles during deformation (dynamic aging), both reducing the mobility of dislocations and, as a result, increasing the Q value [27].

3.5. Deformed microstructures

As-deformed microstructure of the specimen hot-compressed at a strain rate of 0.001 s^{-1} and a deformation temperature of 200 °C is shown in Fig. 7(a). The interfaces of initial powder particles are still recognizable in the deformed microstructure, although almost all of these interfaces are aligned perpendicular to the compression direction, implying the rearrangement and remarkable deformation of powder particles through hot compression. Some porosity is also present in the deformed microstructure.

The etched microstructures of the specimens deformed at a strain rate of 0.001 s^{-1} and at deformation temperatures of 200 °C and 300 °C (corresponding to domain I of the developed processing maps) are shown in Fig. 7(b) and (c) respectively. The microstructure of the specimen deformed at 200 °C (Fig. 7(b)) does not show any sign of dynamic recrystallization, suggesting that dynamic recovery (DRV) is the active restoration mechanism at the lower temperatures of domain I. Nevertheless, the specimen deformed at 300 °C has a fine, equiaxed grain structure (Fig. 7(c)), which confirms the occurrence of dynamic recrystallization (DRX) at the higher temperatures of domain I. The equiaxed grain structure of the specimen deformed at a strain rate of 0.001 s^{-1} and a deformation temperature of 400 °C (Fig. 7(d)) also verifies the occurrence of DRX at this deformation temperature. However, remarkable grain growth suggests that 400 °C is not suitable for hot deformation of AZ91 Mg alloy powder compacts.

As shown above, the restoration mechanism acting in domain I of the developed processing maps is controlled by deformation temperature, and DRX becomes active at the higher temperatures of domain I, which results in a fine, equiaxed grain structure for the specimen deformed at 300 °C and 0.001 s^{-1} (Fig. 7(C)). Moreover, it is reported that a higher deformation temperature develops better bonding between powder particles through hot deformation, which then leads to a better ductility and tensile

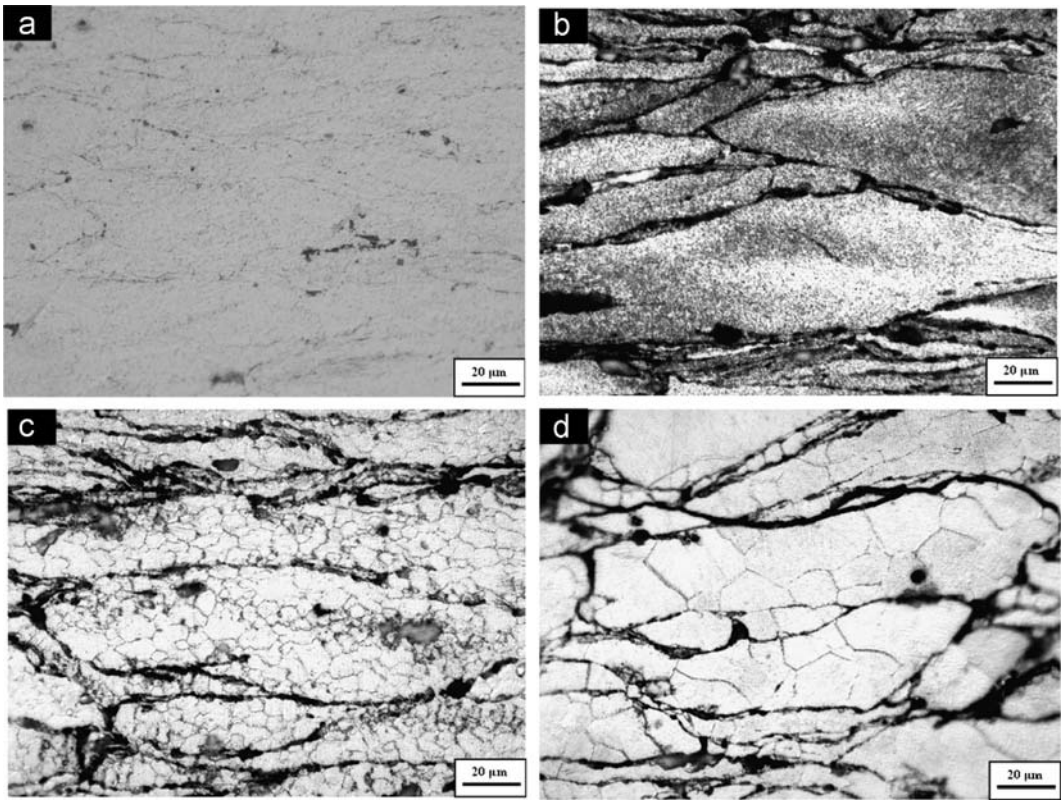

Fig. 7. (a) As-deformed microstructure of the specimen deformed at a strain rate of 0.001 s^{-1} and a deformation temperature of 200 °C. Etched microstructures of the specimens deformed at a strain rate of 0.001 s^{-1} and at deformation temperatures of (b) 200 °C, (c) 300 °C, and (d) 400 °C.

properties for the bulk material consolidated from powder compacts [37]. Considering all above, the optimum condition for hot deformation of AZ91 powder compacts is determined to lie between 275–325 °C and 0.001–0.01 s^{-1}.

4. Conclusions

This research examined the hot deformation behavior and workability characteristics of AZ91 Mg alloy powder compacts with a relative green density of 93% using hot compression tests over a wide range of deformation temperatures and strain rates and a processing map technique. The main conclusions derived from this study are the following:

(1) Strain was found to have important effects on the processing maps of AZ91 Mg alloy powder compacts, although the processing maps developed for different strains had similar features.
(2) The processing maps contained a safe domain for hot deformation, in which the stress–strain curves exhibited a peak, after which the flow stress increased slightly or remained nearly constant.
(3) The value of Q (hot deformation activation energy) calculated for the above-mentioned domain (75 kJ/mol) was lower than those previously reported for the hot compression of bulk AZ91 Mg alloy, which was attributed to the presence of pores in the structure of powder compacts and the starting microstructure of the AZ91 Mg alloy.
(4) The fine, equiaxed grain structure of the specimen deformed at 300 °C and 0.001 s^{-1} confirmed the occurrence of DRX at the higher temperatures of the safe domain for hot deformation. Considering the domain identified in the processing maps and the microstructures of the hot-compressed specimens, the optimum condition for hot deformation of AZ91 powder compacts was determined to lie between 275–325 °C and 0.001–0.01 s^{-1}.

Acknowledgments

The authors would like to thank the Comunidad de Madrid for their financial support of this work through the ESTRUMAT Grant #S2009/MAT-1585.

References

[1] L. Li, M.O. Lai, M. Gupta, B.W. Chua, A. Osman, J. Mater. Sci. 35 (2000) 5553–5561.
[2] H. Ye, X. Liu, J. Mater. Sci. 39 (2004) 6153–6171.
[3] Y.H. Wei, Q.D. Wang, Y.P. Zhu, H.T. Zhou, W.J. Ding, Y. Chino, M. Mabuchi, Mater. Sci. Eng. A 360 (2003) 107–115.
[4] K. Kubota, M. Mabuchi, K. Higashi, J. Mater. Sci. 34 (1999) 2255–2262.
[5] E.F. Volkova, Met. Sci. Heat Treat. 48 (2006) 473–478.
[6] M. Wolff, T. Ebel, M. Dahms, Adv. Eng. Mater. 12 (2010) 829–836.
[7] M. Kulekci, Int. J. Adv. Manuf. Technol. 39 (2008) 851–865.
[8] S.J. Liang, Z.Y. Liu, E.D. Wang, Mater. Lett. 62 (2008) 3051–3054.
[9] B.K. Raghunath, K. Raghukandan, R. Karthikeyan, K. Palanikumar, U.T.S. Pillai, R.A. Gandhi, J. Alloys Compd. 509 (2011) 4992–4998.
[10] K. Ishikawa, H. Watanabe, T. Mukai, Mater. Lett. 59 (2005) 1511–1515.
[11] K. Ishikawa, H. Watanabe, T. Mukai, J. Mater. Sci. 40 (2005) 1577–1582.
[12] C. Zubizarreta, S. Giménez, J.M. Martín, I. Iturriza, J. Alloys Compd. 467 (2009) 191–201.
[13] S. Serajzadeh, A.Karimi Taheri, Mech. Res. Commun. 30 (2003) 87–93.
[14] H. Mirzadeh, A. Najafizadeh, Mater. Sci. Eng. A 527 (2010) 1160–1164.
[15] G. Chunlei, X. Yongdong, W. Mengjun, Mater. Sci. Eng. A 528 (2011) 4199–4203.
[16] H.T. Zhou, Q.B. Li, Z.K. Zhao, Z.C. Liu, S.F. Wen, Q.D. Wang, Mater. Sci. Eng. A 527 (2010) 2022–2026.
[17] S. Anbu Selvan, S. Ramanathan, T. Nonferr. Metal Soc. 21 (2011) 257–264.

[18] N. Srinivasan, Y.V.R.K. Prasad, P.Rama Rao, Mater. Sci. Eng. A 476 (2008) 146–156.
[19] M. yan Zhan, Z. Chen, H. Zhang, W. Xia, Mech. Res. Commun. 33 (2006) 508–514.
[20] M.A. Jabbari Taleghani, E.M. Ruiz Navas, M. Salehi, J.M. Torralba, Mater. Sci. Eng. A 534 (2012) 624–631.
[21] P.T. Wang, M.E. Karabin, Powder Technol. 78 (1994) 67–76.
[22] D. Zhang, S. Wang, C. Qiu, W. Zhang, Mater. Sci. Eng. A 556 (2012) 100–106.
[23] S.W. Xu, N. Matsumoto, S. Kamado, T. Honma, Y. Kojima, Mater. Sci. Eng. A 523 (2009) 47–52.
[24] H. Ding, L. Liu, S. Kamado, W. Ding, Y. Kojima, J. Alloys Compd. 456 (2008) 400–406.
[25] K. Máthis, J. Gubicza, N.H. Nam, J. Alloys Compd. 394 (2005) 194–199.
[26] X.-f. Wang, J.-z. Zhao, J. He, Z.-q. Hu, T Nonferr. Metal Soc. 17 (2007) 238–243.
[27] L. Liu, H. Ding, J. Alloys Compd. 484 (2009) 949–956.
[28] F. Pilehva, A. Zarei-Hanzaki, S.M. Fatemi-Varzaneh, Mater. Des. 42 (2012) 411–417.
[29] Y.V.R.K. Prasad, K.P. Rao, N. Hort, K.U. Kainer, Mater. Lett. 62 (2008) 4207–4209.
[30] P. Changizian, A. Zarei-Hanzaki, H.R. Abedi, Mater. Sci. Eng. A 558 (2012) 44–51.
[31] Z. Li, J. Dong, X.Q. Zeng, C. Lu, W.J. Ding, Mater. Sci. Eng. A 466 (2007) 134–139.
[32] S.W. Xu, S. Kamado, N. Matsumoto, T. Honma, Y. Kojima, Mater. Sci. Eng. A 527 (2009) 52–60.
[33] P. Burke, C. Petit, S. Yakoubi, G.J. Kipouros, Thermal effects of calcium and yttrium additions on the sintering of magnesium powder, Magnesium Technology 2011, John Wiley & Sons, Inc., Hoboken, New Jersey, 481–484.
[34] Y. Deng, Z. Yin, J. Huang, Mater. Sci. Eng. A 528 (2011) 1780–1786.
[35] K.P. Rao, Y.V.R.K. Prasad, Mater. Sci. Eng. A 527 (2010) 6589–6595.
[36] K.P. Rao, Y.V.R.K. Prasad, K. Suresh, Mater. Des. 32 (2011) 4874–4881.
[37] H. Lianxi, L. Zuyan, W. Erde, Mater. Sci. Eng. A 323 (2002) 213–217.